1472 Vol. 57, No. 6 / 20 February 2018 / Applied Optics Research Article

applied optics

Desensitization design method of unobscured three-mirror anastigmatic optical systems with an adjustment-optimization-evaluation process

QINGYU MENG,[1,2,*] HONGYUAN WANG,[1] WEI WANG,[2] AND ZHIQIANG YAN[1]

[1]Research Center for Space Optical Engineering, Harbin Institute of Technology, No. 2 Yikuang Street, Harbin 150001, China
[2]Changchun Institute of Optics, Fine Mechanics and Physics, Chinese Academy of Sciences, No. 3888, Dongnanhu Road, Changchun 130033, China
*Corresponding author: mengqy@ciomp.ac.cn

Received 14 November 2017; revised 15 January 2018; accepted 16 January 2018; posted 19 January 2018 (Doc. ID 313479); published 20 February 2018

An off-axis three-mirror anastigmatic optical system with the offset apertures configuration as a typical unobscured optical system is frequently used in various optical instruments. The practical applications show that this type of system has a higher sensitivity in alignment. To reduce the alignment sensitivity of the unobscured optical systems, a desensitization design method with an adjustment-optimization-evaluation process is proposed. By ray path difference analysis based on the optical system mathematical models, the mirror off-axis magnitude value is determined as a significant factor influencing system alignment sensitivity. Accordingly, in the desensitization design process, the mirror off-axis magnitude value is set as an adjustment, and the image quality and system sensitivity are set as the criteria. By a design example, it proves that the desensitization design method is effective and practical, and the design result sensitivity analysis not only verifies that the off-axis magnitude is a significant factor that influences the system alignment sensitivity, but also finds that there is a positive correlation relation between system sensitivity and off-axis magnitude value. The desensitization method can design the unobscured optical systems with less alignment sensitivity and robust tolerance.

OCIS codes: (220.2740) Geometric optical design; (220.1140) Alignment; (080.4035) Mirror system design.

https://doi.org/10.1364/AO.57.001472

1. INTRODUCTION

Unobscured reflective optical systems have been applied in various optical instruments since the 1960s. This type of optical system wins popularity due to its advantages of a more effective aperture, better spot diagram energy concentration, and improved observation frequency of specified target areas, etc. These characteristics make the unobscured system more competitive than the obscured system. An off-axis three-mirror anastigmatic (TMA) system whose designs emerged in the mid-1970s and began to appear as hardware in the literature in the early 1990s, is a representative frequently used unobscured optical system [1,2].

The off-axis TMA system is an intrinsically rotationally symmetric system that is based on using the off-axis segments of a rotationally symmetric surface, so the TMA's mirrors are the coaxial parent mirrors with the offset apertures. Because of this feature, the mirrors of the off-axis TMA system have faster F-numbers than the mirrors of the coaxial TMA system generally. It is generally known that it is more difficult to fabricate an aspherical mirror with large relative aperture [3,4]. More to the point, the optical system with a faster F-number mirror also has higher alignment sensitivity. In the optical system manufacturing process, the optical system alignment sensitivity is positively associated with the cost and duration. So, no matter from the technical points or the economical points, it is of great significance to design an unobscured optical system with less alignment sensitivity. In recent decades, unobscured TMA systems have been more and more applied in optical remote sensors. To obtain high resolution, the optical systems (usually with long focal length) have large scale with high cost. Our main research purpose is to reduce the alignment sensitivity of this category of the unobscured TMA system.

Decreasing the number of alignment degrees of freedom (DOFs) of an optical system is a direct means of reducing alignment difficulty. Once we have designed an off-axis TMA system with an integration of the primary mirror (PM) and tertiary mirror (TM) using freeform surfaces, due to the ability of the PM and TM to be integrated as a monolithic mirror in the design process, the system alignment DOF is reduced from 12 to 6, which is benefited from the decrease of the number of mirrors. Consequently, the system alignment difficulty is reduced [5,6]. A low F-number freeform off-axis TMA system with an integration mirror is also designed and manufactured, and the system alignment DOF can also be reduced [7,8]. With the similar design concept, a four-mirror optical system in which the PM and the TM and the secondary mirror (SM) and the quaternary mirror are monolithically fabricated on two common mirror bodies respectively has been achieved. The alignment effort is reduced by arranging two optical surfaces monolithically on common mirror bodies [9,10]. The integration mirror design philosophy has been researched deeply and remarkable achievements have been achieved [10–17]. However, the easy-alignment method by the integration mirror just only can reduce the system alignment DOF, but it cannot reduce the system alignment sensitivity from system properties. One of the representative achievements in the reduction of optical system alignment sensitivity is an unobscured, $F/1.9$, 10° full field of view (FOV) long-wave infrared imager, and the mechanism of its lower alignment sensitivity compared with a traditional unobscured TMA (Cook TMA) has been analyzed by the nodal aberration theory qualitatively [18,19]. In addition, a design of an unobscured organic light emitting diode (OLED)-based reflective freeform electronic viewfinder covering a 25° full FOV with a 12 mm eyebox has been achieved [20], and the analysis shows that this system has a potential low alignment sensitivity; however, no more detailed design method is introduced.

In this paper, the factor that influences the alignment sensitivity of the unobscured optical systems is analyzed, and based on the analysis guidance, we present a desensitization design method of the unobscured TMA optical systems with an adjustment-optimization-evaluation (AOE) process. The design method can guide people to more easily achieve an unobscured system with less alignment sensitivity.

First, to explore the alignment sensitivity factor of the unobscured systems, the optical system mathematical models have been established. By the ray-tracing method, we obtain the characteristic mathematical relation of the ray path length (RPL) both in the original condition and misalignment condition [21]. The ray path difference (RPD) and root mean square (RMS) RPDs caused by the misalignment are taken as the optical alignment sensitivity evaluation criteria respectively, and a conclusion is drawn that the system mirror off-axis magnitude (OM) is a significant factor influencing the system alignment sensitivity, and this sensitivity factor is positively correlated with OM.

Second, the desensitization design method of the unobscured TMA optical systems with the AOE process is proposed. In this method, the OM is set as an adjustment, and the system alignment sensitivity and image quality are set as the criteria. During the design process, the iterations of OM adjustment correction, image quality evaluation, and sensitivity analysis are used to achieve an unobscured optical system with a lower and acceptable sensitivity.

Third, to verify the correctness and practicability of the mathematical derivation of the system alignment sensitivity factor, and the effectiveness of the AOE desensitization design method, a design example is given. By sensitivity analysis, it not only proves the effectiveness of the AOE iteration desensitization design method, but also reveals that the system alignment sensitivity is the positive correlation relation with the OM value.

Upon comprehensive analysis, the AOE desensitization design method is effective and practical to design the unobscured TMA optical systems with lower alignment sensitivity.

2. ALIGNMENT SENSITIVITY FACTOR ANALYSIS AND THE AOE DESENSITIZATION DESIGN METHOD

Any optical element misalignments will lead to the degeneration of the imaging quality. The misalignments will break the optical system aberration field balance and derive system wavefront distortion. A robust tolerance optical system can well resist the harmful effect that is caused by the element misalignments, and in other words, the element position changes bring smaller influence on the optical system. This robust tolerance optical system is our desired system [22].

For this purpose, in this section, we will analyze the optical element misalignment from the perspective of basic ray tracing, and take the RPD and RMS RPDs caused by the misalignment as the optical alignment sensitivity evaluation criteria. Based on the analysis, we seek the factor influencing the alignment sensitivity of the off-axis unobscured optical system, and then apply the conclusion to develop a desensitization design method to achieve the unobscured TMA optical systems with low sensitivity in alignment.

A. Mathematical Model Establishment

The ray-tracing mathematical model is a simplified one-mirror off-axis system, as shown in Fig. 1. It uses right-handed optical coordinates, and the nominal optical axis is the z-axis. The $+y$-axis is "up," and the $+x$-axis is toward the left. In the model system, D is the aperture and h is the mirror OM.

The mirror surface is set as a sphere, the aperture center axis is parallel to the optical axis, and the form is as follows:

$$z = \frac{cr^2}{1 + \sqrt{1 - c^2 r^2}}, \quad (1)$$

where z is the sag of the surface parallel to the z-axis, c is the curvature at the pole of the surface, and r is the radial distance. The mirror surface also can be simplified and expressed in polar coordinate as

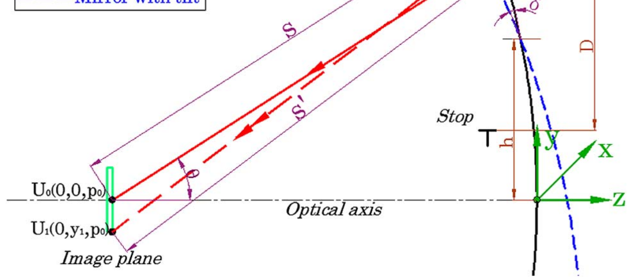

Fig. 1. Ray-tracing mathematical model.

$$z = z(r). \tag{1a}$$

First, the RPL between object point O_0 and image point U_0 is calculated. Here, we just take an example of the on-axis ray from O_0 for analysis as a typical condition. Object point O_0 coordinates are (x_0, y_0, z_0), and the intersection point coordinates of the incident ray on the mirror are $O(x, y, z)$. Depending on the law of reflection,

$$\mathbf{I} \times \mathbf{N} = \mathbf{R} \times \mathbf{N}, \tag{2}$$

where $\mathbf{I}$, $\mathbf{R}$ are the unit vectors along the directions of the incident and exit rays, respectively. $\mathbf{N}$ is the normal vector:

$$\mathbf{I} = (\,0, \quad 0, \quad 1\,), \tag{3}$$

$$\mathbf{N} = \left(-\tfrac{\partial z}{\partial x}, \quad -\tfrac{\partial z}{\partial y}, \quad 1\right) = (\,-z_x, \quad -z_y, \quad 1\,). \tag{4}$$

And then the exit unit vector $\mathbf{R}$ is express as

$$\mathbf{R} = \frac{1}{S}(\,-x, \quad -y, \quad p_0 - z\,). \tag{5}$$

In unit vector $\mathbf{R}$, p_0 are the intersection point coordinates of the exit ray with the optical axis in the z-axis direction. We also define p_0 as the intersection point coordinates of the image plane with the optical axis. S is the length between point O and point $U_0(0, 0, p_0)$:

$$S = \sqrt{x^2 + y^2 + (p_0 - z)^2}. \tag{6}$$

From Eqs. (2)–(6), we can obtain the relation as Eq. group (7):

$$\begin{cases} z_x = x/(p_0 - z - S) \\ z_y = y/(p_0 - z - S)\,. \\ \quad z_x/z_y = x/y \end{cases} \tag{7}$$

Mirror angular misalignment is a typical misalignment condition of an optical system, and next we will take this condition as a representation to analyze the optical system alignment sensitivity factor. When the mirror generates an angular misalignment, the mirror is assumed to rotate about the intersection between the aperture center axis and the mirror surface, and it generates a tilt of δ. The mirror surface form is as follows:

$$z = z(r) + (y - h)\delta. \tag{8}$$

Here we made a small angle approximation by using δ instead of $\sin\delta$, and this term is much smaller than the original surface shape.

In this condition, the intersection point coordinates of the incident ray on the mirror are $O'(x', y', z')$. The intersection point coordinates of the exit ray on the image plane are $U_1(0, y_1, p_0)$. Here, the new normal vector $\mathbf{N}'$ is

$$\mathbf{N}' = (\,-z_{x1}, \quad -z_{y1}, \quad 1\,). \tag{9}$$

$\mathbf{I}'$ is the unit vector along the directions of the incident ray, and $\mathbf{I}' = \mathbf{I}$, depending on the law of reflection:

$$\mathbf{I}' \times \mathbf{N}' = \begin{vmatrix} \mathbf{i} & \mathbf{j} & \mathbf{k} \\ 0 & 0 & 1 \\ -z_{x1} & -z_{y1} & 1 \end{vmatrix} = \begin{pmatrix} z_{y1} \\ -z_{x1} \\ 0 \end{pmatrix}. \tag{10}$$

So, the unit vector along the directions of the exit ray $\mathbf{R}'$ can be expressed as

$$\mathbf{R}' = \frac{1}{S'}(\,-x, \quad y_1 - y, \quad p_0 - z'\,). \tag{11}$$

S' is the length between point O' and point U_1. Similar with the previous mathematical derivation, we can obtain the mathematical relation as Eq. (11):

$$\begin{aligned} \mathbf{R}' \times \mathbf{N} &= \frac{1}{S'}\begin{vmatrix} \mathbf{i} & \mathbf{j} & \mathbf{k} \\ -x & y_1 - y & p_0 - z' \\ -z_{x1} & -z_{y1} & 1 \end{vmatrix} \\ &= \frac{1}{S'}\begin{pmatrix} y_1 - y + z_{y1}(p_0 - z') \\ -z_{x1}(p_0 - z') + x \\ xz_{y1} + z_{x1}(y_1 - y) \end{pmatrix}. \end{aligned} \tag{12}$$

Depending on the law of reflection and Eqs. (10)–(12), we can get Eq. (13):

$$y_1 = y - \frac{z_{y1}}{z_{x1}}x. \tag{13}$$

Here, we decompose z_{y1} into z_y and the derivative of $(y - h)\delta$ as

$$z_{y1} = z_y + z_{y\delta}. \tag{14}$$

Because $z_x = z_{x1}$, and according to Eq. group (7) and Eq. (14), Eq. (13) can be expressed as

$$y_1 = -(p_0 - z - S)\delta. \tag{15}$$

We define the $(S + p_0 - z)$ as a factor that is expressed by M:

$$y_1 = -M\delta. \tag{16}$$

Based on the above analyses, the characteristic mathematical relation of the ray both in the original condition and misalignment condition has been derived and confirmed.

B. Calculation of RPD for the System with Misalignment Perturbation

The RPD is defined as the difference between the RPL of a single ray before the perturbation to that after the perturbation. As mentioned above, the RPD is taken as the optical alignment sensitivity evaluation criterion. When the optical element generates position perturbation, the optical system with higher alignment sensitivity will generate larger RPD than the optical system with less alignment sensitivity.

Based on the previous analysis, when the optical system in the original condition, the RPL from the object point O_0 to the image point U_0 is

$$\mathrm{RPL}(\overline{O_0 O U_0}) = z - z_0 + S. \tag{17}$$

When the optical system mirror generates angular misalignment, the RPL from the object O_0 to the new image point U_1 is

$$\mathrm{RPL}'(\overline{O_0 O' U_1}) = z' - z_0 + S'. \tag{18}$$

Following, combined with Eqs. (7) and (16), Eq. (18) can be approximately expressed as Eq. (19):

$$\begin{aligned}\mathrm{RPL}' &= z' - z_0 + S' \\ &= z + (y-h)\delta - z_0 + \sqrt{x^2 + (y_1 - y)^2 + (p_0 - z')^2} \\ &= z - z_0 + (y-h)\delta + \sqrt{\begin{aligned}& x^2 + y^2 + p_0^2 + y_1^2 + \underbrace{[z + (y-h)\delta]^2}_{z'^2} \ldots \\ & -2p_0\underbrace{[z + (y-h)\delta]}_{z'} - 2yy_1\end{aligned}} \\ &= z - z_0 + (y-h)\delta + \sqrt{\begin{aligned}& x^2 + y^2 + p_0^2 + z^2 + 2z(y-h)\delta - 2p_0 z \ldots \\ & -2p_0(y-h)\delta + 2yM\delta + \underbrace{y_1^2 + (y-h)^2\delta^2}_{o(\delta^2)}\end{aligned}}.\end{aligned} \tag{19}$$

Neglecting the second-order small quantities of δ, Eq. (19) can be expressed as

$$\mathrm{RPL}' \approx z - z_0 + (y-h)\delta + S\sqrt{1 + 2\delta\frac{(y-h)(z-p_0) + yM}{S^2}}. \tag{19a}$$

By using the first-order approximation of the Taylor expansion, Eq. (19a) can be expressed as Eq. (20):

$$\begin{aligned}&\mathrm{RPL}'(\overline{O_0 O' U_1}) \\ &\approx z - z_0 + (y-h)\delta + S + \frac{(y-h)(z-p_0)}{S}\delta + \frac{My}{S}\delta.\end{aligned} \tag{20}$$

Based on the above derivations, the RPD caused by the misalignment is

$$\begin{aligned}\mathrm{RPD} &= \mathrm{RPL}'(\overline{O_0 O' U_1}) - \mathrm{RPL}(\overline{O_0 O U_0}) \\ &= \left\{z - z_0 + (y-h)\delta + S + \frac{(y-h)(z-p_0)}{S}\delta + \frac{yM}{S}\delta\right\}\ldots \\ &\quad - (z - z_0 + S) \\ &= h\delta\frac{p_0 - z}{S} - h\delta \\ &= -h\delta(1 + \cos\theta).\end{aligned} \tag{21}$$

θ is the included angle between exit ray $\overrightarrow{OU_0}$ and optical axis z, shown in Fig. 1.

Equation (21) illustrates that the OM is a significant factor that influences the unobscured system alignment sensitivity, and this factor is positively correlated with the OM value.

Angular misalignment is a typical and major misalignment in an optical system, although only the typical mirror angular misalignment in the x direction (tilt-x) has been analyzed for the system sensitivity factor; it can demonstrate the positive correlation between the system OM and alignment sensitivity qualitatively.

As mentioned in the start of this section, the RPD is defined as the difference between the RPL of one single ray before the perturbation to that after the perturbation. The definition illustrates that, in the RPD calculation, the reference ray is the ray itself before perturbation, and is not other rays, such as the paraxial ray. So, this mathematical model avoids the interference of ray aberration. It is more convenient for the sensitivity factor research.

C. Calculation of RMSRPDs for the System with Misalignment Perturbation

In Section 2.B, the RPD in two-dimensional space is taken to be researched for the alignment sensitivity factor. In this section, the symmetric sampling of the mirror (pupil) by more rays will be analyzed to evaluate the alignment sensitivity factor.

The mean square value of the optical path difference (OPD) and the variance of the OPD can be used to evaluate the image quality [23,24]. Similarly, the RMS RPDs is introduced to evaluate the system alignment sensitivity. The system with higher alignment sensitivity will generate a larger RMS RPD when it is with misalignment perturbation.

The RMS RPD is marked as Φ and is defined as

$$\Phi^2 = \frac{1}{A}\iint (\mathrm{RPD})^2 \mathrm{d}A. \tag{22}$$

The two-dimensional mathematical model in Fig. 1 is extended to three-dimensional space, which is shown in Fig. 2. The intersection point coordinates $O(x, y, z)$ of the incident ray on the mirror (pupil) are expressed in polar coordinates as

$$\begin{cases} x = \rho\cos\varphi \\ y = \rho\sin\varphi + h' \end{cases} \tag{23}$$

where ρ denotes the mirror (pupil) polar radius, which ranges from 0 to R, and φ denotes the polar angle, which ranges from 0 to 2π.

Based on Eq. (21), the relation between the RPD and Φ is expressed as Eq. (24), and A is the integral area (mirror area):

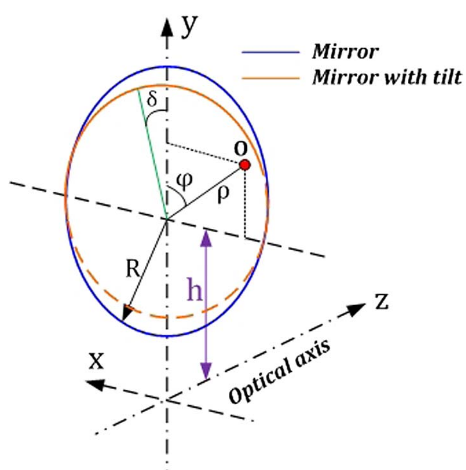

Fig. 2. Three-dimensional space ray-tracing mathematical model.

$$\Phi^2 = \frac{1}{A}\iint h^2\delta^2(1+\cos\theta)^2\mathrm{d}A$$
$$= \frac{h^2\delta^2}{A}\iint(1+2\cos\theta+\cos^2\theta)\mathrm{d}A. \quad \textbf{(24)}$$

We define the core part of Eq. (24) as ξ, shown in Eq. (25):

$$\xi = \iint(1+2\cos\theta+\cos^2\theta)\mathrm{d}A. \quad \textbf{(25)}$$

Based on the Taylor approximation as Eq. (26):

$$\cos\theta \approx 1-\frac{1}{2}\theta^2 \approx 1-\frac{1}{2}\sin^2\theta. \quad \textbf{(26)}$$

The ξ can be expressed as

$$\xi = \iint(1+2\cos\theta+\cos^2\theta)\rho\mathrm{d}\rho\mathrm{d}\varphi$$
$$= 4\iint\rho\mathrm{d}\rho\mathrm{d}\varphi - 2\iint\sin^2\theta\rho\mathrm{d}\rho\mathrm{d}\varphi. \quad \textbf{(27)}$$

Known from Fig. 1, there is a mathematical relation:

$$\sin\theta = \frac{\sqrt{x^2+y^2}}{\sqrt{x^2+y^2+(p_0-z)^2}}$$
$$= \frac{\sqrt{(\rho\cos\varphi)^2+(\rho\sin\varphi+h)^2}}{\sqrt{(\rho\cos\varphi)^2+(\rho\sin\varphi+h)^2+(p_0-z)^2}}. \quad \textbf{(28)}$$

As mentioned in the introduction, we are more focused on the desensitization of the high-resolution unobscured TMA systems in large scale. Among the commonly used unobscured TMA systems, especially in a visible band optical remote sensor, such as the off-axis Cook TMA (the entrance pupil at the PM, and with relay image plane), we make the following assumptions:

(i) The focal length of the mirror is much larger than the sag of the mirror surface parallel to the optical axis, and this is true in most reflection systems.

(ii) The square of the focal length is much larger than the square of the OM. We should note that we did not assume the focal length is much larger than the OM, since it is not always true as well as it is not necessary for the derivation below. Generally, the PM F-number is about or larger than 3, and the OM value is approximately in the value of the mirror aperture. So the focal length is several times larger than the OM, and the square of the focal length will be more than 10 times larger than the square of the OM.

(iii) Based on the previous assumption, the focal length is several times larger than ρ, and the square of the focal length will be over 10 times larger than the square of ρ.

So, there are the mathematical relations as

$$\begin{cases} p_0 \gg z \\ p_0^2 \gg h^2 \\ p_0^2 \gg \rho^2 \end{cases}. \quad \textbf{(29)}$$

Although the assumptions in Eq. (29) have some certain limitations, they are meaningful for the alignment sensitivity analysis of the high-resolution unobscured TMA systems in large scale.

Based on the assumptions in Eq. (29), Eq. (28) is expressed as Eq. (30):

$$\sin\theta \approx \frac{\sqrt{\rho^2+h^2+2\rho h\sin\varphi}}{\sqrt{\rho^2+h^2+2\rho h\sin\varphi+p_0^2}} \approx 0. \quad \textbf{(30)}$$

In the calculation process, based on the assumption $p_0 \gg z$ in Eq. (29), we use p_0 instead of $(p_0 - z)$ in Eq. (28). And based on the assumptions $p_0^2 \gg h^2$ and $p_0^2 \gg \rho^2$ in Eq. (29), Eq. (28) is approximately equal to zero.

The calculation results of ξ is

$$\xi = \iint(1+2\cos\theta+\cos^2\theta)\rho\mathrm{d}\rho\mathrm{d}\varphi$$
$$= 4\iint\rho\mathrm{d}\rho\mathrm{d}\varphi - 2\iint\sin^2\theta\rho\mathrm{d}\rho\mathrm{d}\varphi$$
$$\approx 4\pi R^2. \quad \textbf{(31)}$$

The RMS RPDs Φ is

$$\Phi = \frac{h\delta}{\sqrt{A}}\sqrt{\xi} = 2h\delta. \quad \textbf{(32)}$$

Based on the above quantitative analysis and the conclusive equation shown in Eq. (32), it illustrates that the OM is a significant factor influencing on the unobscured system alignment sensitivity, and the RMS RPDs Φ is positively correlated with the OM. This conclusion provides the theoretical basis for the system alignment sensitivity factor and will guide us to develop the practical desensitization design method.

Two simple optical systems comparisons can illustrate the conclusion simply and clearly. System I and system II are the two simple optical systems, which are shown in Fig. 3, and they are all off-axis one-parabolic-mirror systems that have the same aperture of Φ100 mm, the same F-number of 5, and the same FOV of 0°. The OM value of system I is 100 mm, and the OM value of system II is 150 mm. When the mirror generates an angular misalignment, the mirror is assumed to

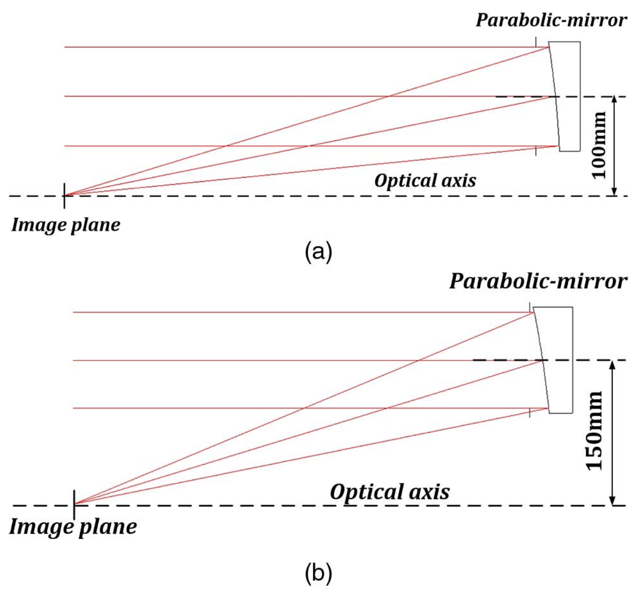

Fig. 3. Off-axis one-parabolic-mirror systems: (a) system I with OM 100 mm, (b) system II with OM 150 mm.

rotate about the intersection between the aperture center axis parallel to the optical axis and the mirror surface, and it generates a tilt of δ, which is set to 10 in. In the misalignment condition, the RMS wavefront error (WFE) of system I is 0.06030λ ($\lambda = 632.8$ nm), and the RMS WFE of system II is 0.08797λ. The simple comparisons are conducive to understanding the sensitivity factor and developing an optical system desensitization design method.

D. Desensitization Design Method for the Unobscured TMA Systems with Low Alignment Sensitivity

Based on the above analyses from multiple perspectives in Sections 2.B and 2.C, the OM has been identified as a significant factor influencing the system alignment sensitivity. To decrease the unobscured TMA system alignment sensitivity, an AOE desensitization design method is proposed here.

In this method, the OM is set as an adjustment, and the system sensitivity and image quality are set as the criteria. During the design process, the iterations of OM adjustment correction, image quality evaluation, and sensitivity analysis are used to achieve an unobscured optical system with a lower and acceptable sensitivity. The brief design flow is as follows:

i. Generally, an unobscured TMA system begins with solving the initial structure of a coaxial TMA system; therefore, the approaches in which using the offset aperture or the offset FOV are adopted before system optimization to avoid ray-tracing obscuration.

For the coaxial nonrelayed TMA optical system, the FOV offset method is commonly adopted to establish an unobscured off-axis nonrelayed TMA, and the aperture offset method is also adopted as the auxiliary method. For the coaxial relayed TMA optical system, the aperture offset method is commonly adopted to establish an unobscured off-axis nonrelayed TMA, and the FOV offset method is also adopted as the auxiliary method. The scheme of the establishment method of the unobscured TMA system from the coaxial TMA system is shown in Fig. 4.

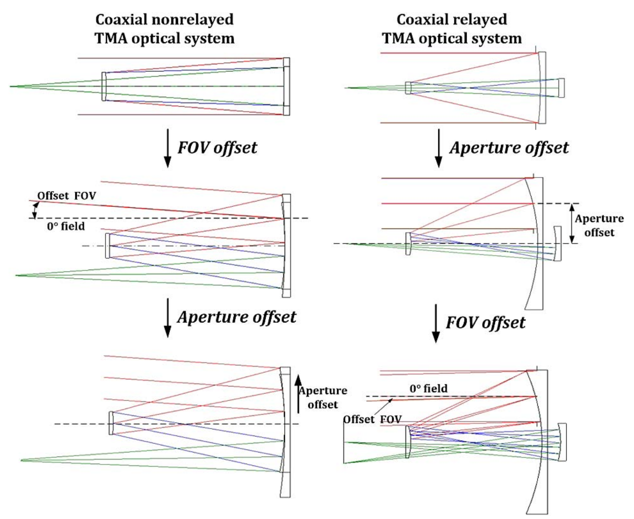

Fig. 4. Scheme of the establishment method of the unobscured TMA system from the coaxial TMA system.

ii. During the optimization process, the ray direction will be modulated with the changes of the surface parameters, such as radius, aspherical parameters, and so on. To avoid obscuration, the system OM or FOV range are set as the adjustments in the optimization process, and the mirror position, such as tilt and decentration, also can be set as a set of adjustment options to eliminate obscuration. The stage design results should guarantee the image quality requirement and no obscuration in the system.

iii. After each stage design, the system alignment sensitivity whose thresholding can be set beforehand should be analyzed and evaluated. If the sensitivity is too high to accept, the system should repeat the iterations in the process of adjustment optimization. The system can be confirmed when the sensitivity is acceptable.

In the AOE design process, the "image performance" can be evaluated by the system RMS WFE, and "obscuration judgment" is judged that whether there is ray obscuration caused by mirror or ray crossing.

The sensitivity evaluation criterion we adopted is the derivative with respect to "misalignment perturbations of each mirror" of the "system RMS WFE." The sensitivity evaluation criterion is defined as

$$\mathrm{Sen} = \frac{\mathrm{d}W}{\mathrm{d}M}, \tag{33}$$

where W is "system RMS WFE," and M is "misalignment perturbations of each mirror." In addition, a variety of sensitivity evaluation criteria can be defined by the designer, for example, the "derivative increments" in CODE V also can represent the

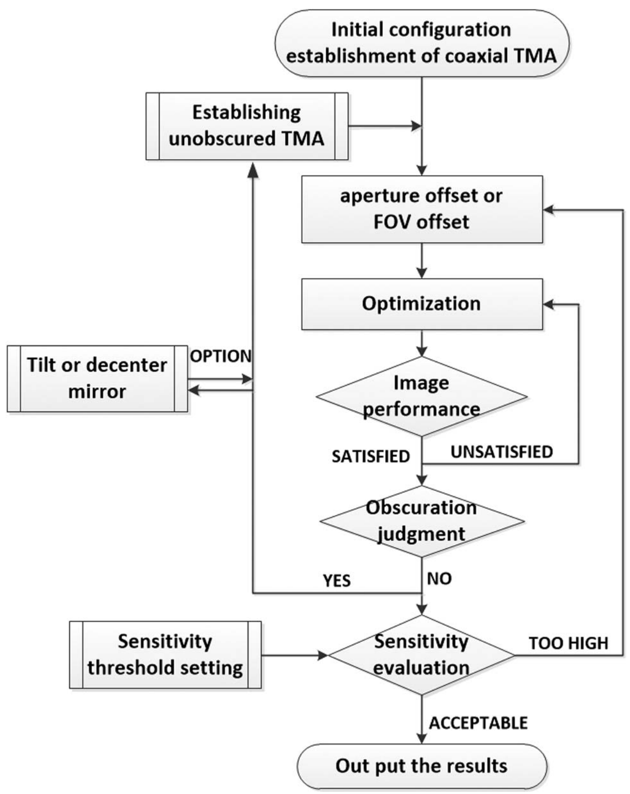

Fig. 5. Flow diagram of the desensitization design method for the unobscured TMA system with lower alignment sensitivity.

system alignment sensitivity to some extent. Sensitivity thresholding is set based on Eq. (33), and the acceptability is decided by the designer or consumer on the basis of its engineering capability.

The above AOE desensitization iteration design method can be operated with the help of data interchange between CODE V and data processing software [25], and the desensitization design process will be efficient.

The flow diagram of the desensitization design method for the unobscured TMA system with low sensitivity in alignment is shown in Fig. 5.

3. DESIGN EXAMPLE AND SENSITIVITY ANALYSIS OF THE UNOBSCURED TMA SYSTEMS BY THE AOE DESENSITIZATION DESIGN METHOD

A. Design Example by the AOE Desensitization Design Method

As an example and verification, an unobscured TMA system is designed with the desensitization design method. The system has a focal length of 3600 mm, an F-number of 15, and a rectangle FOV of $2° \times 1°$, of which the tangential direction (y direction) FOV is $\pm 0.5°$ and the sagittal direction (x direction) FOV is $\pm 1.0°$.

The design process is under the guidance of the AOE desensitization design method. Four representative stage design results are given out to state the AOE method.

First, an initial coaxial TMA system is established, which is shown in Fig. 6(a). The initial TMA configuration can be solved by third-order aberration, and it also can be obtained by private lens catalog [5,6]. To establish the unobscured TMA system configuration, 350 mm OM value (artificial setting value) is added on the initial coaxial system, and we mark it as "system A," which is shown in Fig. 6(b). By optimization, the "system A" has a RMS WFE average value of 0.0250λ ($\lambda = 0.6328$ μm).

By sensitivity analysis and evaluation, it is found that the system alignment sensitivity is high and it can be reduced as the OM value decreases. By constant adjustment optimization, the system OM value is adjusted to 250 mm and the new system is marked as "system B," shown in Fig. 6(c). By optimization, the system has a RMS WFE average value of 0.0195λ ($\lambda = 0.6328$ μm).

To further reduce the system alignment sensitivity, which is a positive correlation of the OM, the OM value is set to 200 mm to obtain a new system marked as "system C." However, although the sensitivity has been further reduced due to the OM value decrease, in "system C," the SM has the aperture obscuration to the ray in the back focal length region, as shown in Fig. 6(d). In addition, ray crossing exists around the region of the relay image plane and the exit pupil, and it is not beneficial to set a diaphragm or folding mirror in such a case. So, the "system C" is an unpractical system.

To remove the ray obscuration and ray crossing while also keeping the system with a small OM value, the TM has been tilted for a minor angle in the adjustment process, then the new system is marked as "system D," shown in Fig. 6(e). Tilt and decentration will derive asymmetric aberrations, which will make the system more difficult to achieve a good imaging quality. To eliminate and balance system aberration, optical freeform surfaces that have strong aberration correction ability have been applied in the TM of "system D" [26–28]. Freeform surfaces are defined as non-rotationally symmetric surfaces and

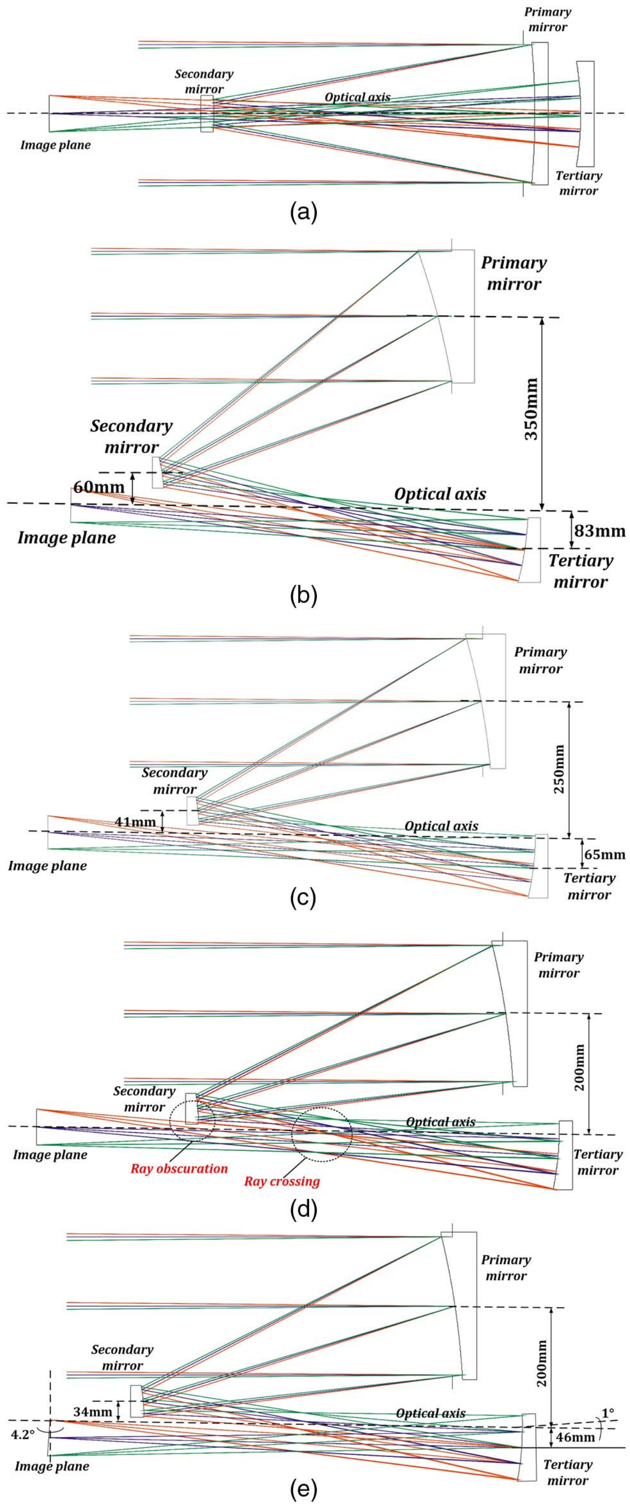

Fig. 6. Off-axis TMA system design comparison: (a) initial coaxial TMA system, (b) system A with OM 350 mm, (c) system B with OM 250 mm, (d) system C with OM 200 mm, (e) system D with OM 200 mm, TM and image plane with tilt.

offer more DOFs in the optical optimization process [29,30]. The mathematical descriptions of freeform surfaces are diversified [31,32]. Here, the Fringe Zernike polynomial is selected as the optical freeform in the TM of "system D." During the optimization process, the freeform polynomial coefficients are distributed and adjusted under the guidance of quantitative and qualitative relations between the freeform polynomial coefficients and aberrations [6,33].

By AOE method iteration, the "system D" has a RMS WFE average value of 0.0200λ ($\lambda = 0.6328$ μm), and its sensitivity is acceptable, which is lower than "system A" and "system B."

The detailed sensitivity will be analyzed in the next section. The configuration parameters and surface parameters of system A, system B, and system D are given in Tables 1–4.

Need of note are that, during the optimization process, the system focal length is set as the constraint, and the system RMS WFE is set as the imaging quality evaluation criterion. Only the OM is set as a main adjustment, and the other parameters, such as the mirror focal power, the distance between each mirror of each system, and the surface parameters, are almost unchanged or have minor adjustments. So, the design results and analyses are beneficial to distinguishing whether the OM acts as a significant factor that influences the system alignment sensitivity.

B. Analysis of the System Alignment Sensitivity

During the AOE method iteration, the goal system is evolved from "system A" to "system D." To keep the TMA systems having good relative property and strong contrast, each mirror in these systems has almost the same focal power distributions. To show the effectiveness of the AOE iteration desensitization design method, more detailed alignment sensitivity analyses are conducted in this section. The relations between system RMS WFE and misalignment perturbations of each mirror of each system have been given.

The typical position misalignments (x-tilt, y-tilt, rotation, x-decenter, y-decenter) are perturbed a specified amount on

Table 1. Configuration Parameters of System A

	Surface Type	Radius (mm)	Thickness (mm)	H (mm)	Optical Overall Dimension (mm)
PM	Conic	–1338.86	–557.59	350.00	Φ240
SM	Conic	–371.67	680.88	60.00	62 × 55
TM	Conic	–545.32	–856.30	–83.00	172 × 116

Table 2. Configuration Parameters of System B

	Surface Type	Radius (mm)	Thickness (mm)	H (mm)	Optical Overall Dimension (mm)
PM	Conic	–1332.00	–558.70	250.00	Φ240
SM	Conic	–380.60	638.60	41.00	60 × 52
TM	Conic	–551.40	–925.88	–65.00	170 × 117

Table 3. Configuration Parameters of System D

	Surface Type	Radius (mm)	Thickness (mm)	H (mm)	Optical Overall Dimension (mm)
PM	Conic	–1336.59	–556.82	200.00	Φ240
SM	Conic	–373.10	659.16	34.00	61 × 52
TM	Conic	–523.34	–823.29	–46.00	168 × 112

Table 4. Surface Parameters of System A, System B, and System D

	Parameters		System A	System B	System D
PM	Conic		–0.9509	–0.9518	–0.9582
SM	Conic		–4.3945	–5.3057	–4.4802
TM	Conic		–0.3901	–0.3875	–0.3486
	Fringe Zernike Polynomial	Z5	Null	Null	–0.0093
		Z6			–2.3918e – 10
		Z7			–2.3203e – 11
		Z8			0.0058
		Z9			0.0012
		Z10			2.2768e – 10
		Z11			3.3869e – 05

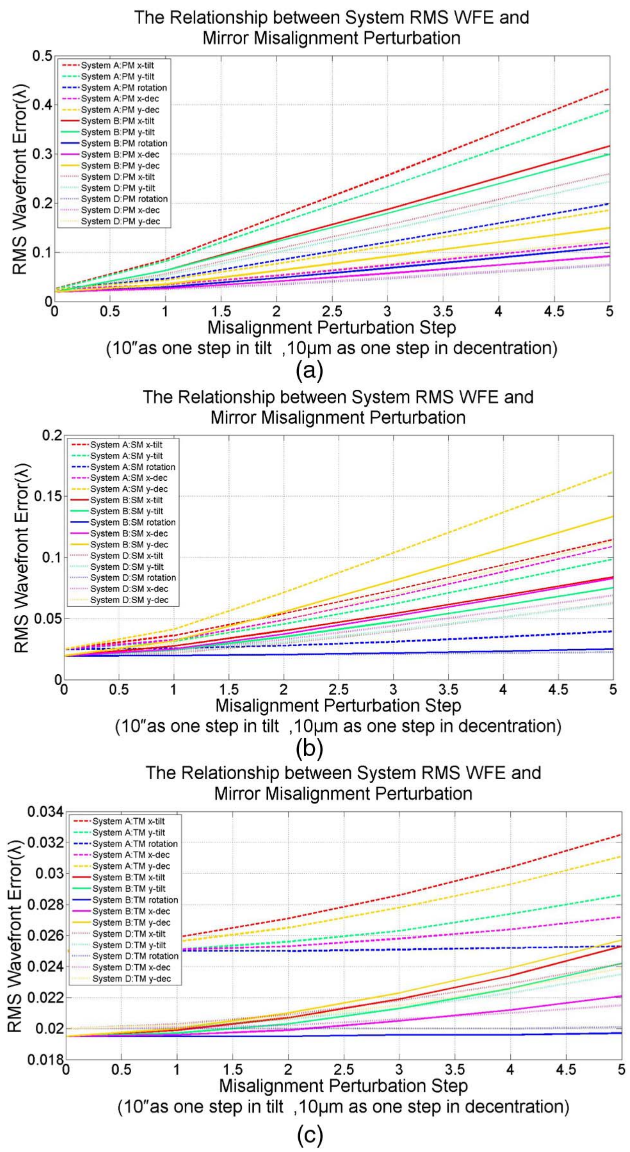

Fig. 7. Relation between system RMS WFE and misalignment perturbations of each mirror: (a) PM, (b) SM, (c) TM for each system.

the mirrors [34]. 10 arc sec and 10 μm are as one step length for angle and displacement misalignment perturbation, respectively. The total step value is set to 5 [19]. The change rate of the system RMS WFE is taken as the alignment sensitivity evaluation criterion. There is no compensator in the perturbation process, so the results also can represent the system stability. The relation between system RMS WFE and each mirror misalignment perturbation is shown in Fig. 7. The data of alignment sensitivity analyses of "system A," "system B," and "system D" are shown in Table 5.

As can be seen from Fig. 7, when each mirror has the same value of misalignment perturbation, the rank of the change ratio of the system RMS WFE from high to low is almost system A, system B, and system D.

The absolute increment of the system RMS WFE caused by each mirror maximum misalignment perturbation (50 in. in angle, 50 μm in displacement) is calculated in Table 5, and the corresponding statistical histograms are shown in Fig. 8.

The analyses clearly show that the alignment sensitivity rank from high to low is system A, system B, system D, and the sequence is positively associated with the OM value. The result not only can verify the correctness of the conclusion that the OM is a significant factor that influences the system alignment sensitivity, but also can verify the effectiveness of the AOE desensitization design method.

Furthermore, it is found that there is an approximate equal proportion relation between the total absolute increment of the system RMS WFE caused by each mirror synthetical misalignment perturbation of each optical system and the each mirror OM value, as shown in Table 6. The relation once again verifies that the OM as a significant factor that influences the unobscured system alignment sensitivity, and it also can help the designer master the sensitivity characteristic during the system design process.

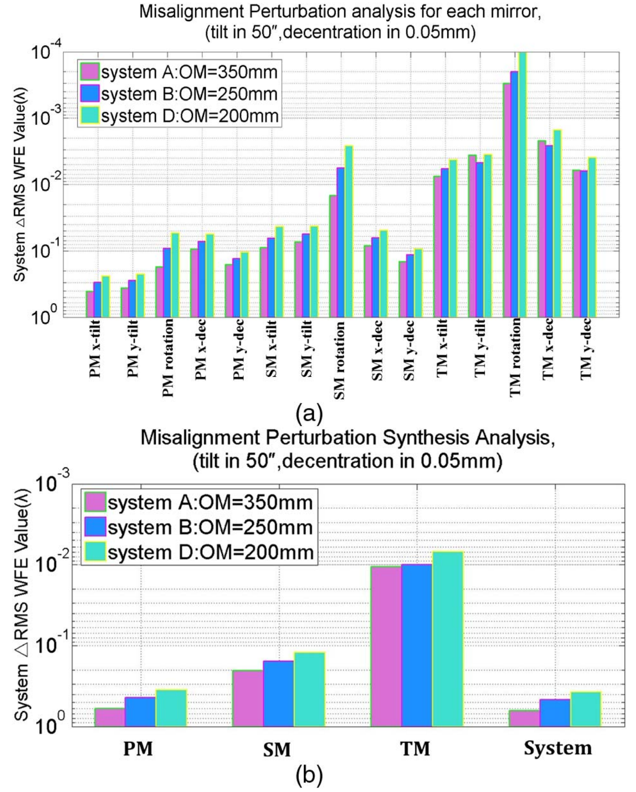

Fig. 8. System RMS WFE increment caused by misalignment perturbations of the three off-axis TMA systems: (a) individual perturbation analysis, (b) synthesis perturbation analysis.

Table 5. Alignment Sensitivity Analyses of Unobscured Systems[a]

Tolerance	Value	System ΔRMS WFE (λ) System A	System B	System D
Primary Mirror (PM)				
x-tilt	50 in.	0.4081	0.2963	0.2395
y-tilt	50 in.	0.3639	0.2795	0.2238
Rotation	50 in.	0.1741	0.0912	0.0536
x-decenter	50 μm	0.0938	0.0724	0.0557
y-decenter	50 μm	0.1607	0.1303	0.1047
PM synthetical ΔRMS WFE (λ)		**0.6032**	**0.4432**	**0.3527**
Secondary Mirror (SM)				
x-tilt	50 in.	0.0897	0.0645	0.0428
y-tilt	50 in.	0.0735	0.0557	0.0421
Rotation	50 in.	0.0146	0.0056	0.0026
x-decenter	50 μm	0.0840	0.0634	0.0490
y-decenter	50 μm	0.1449	0.1138	0.0929
SM synthetical ΔRMS WFE (λ)		**0.2042**	**0.1558**	**0.1210**
Tertiary Mirror (TM)				
x-tilt	50 in.	0.0075	0.0058	0.0042
y-tilt	50 in.	0.0036	0.0047	0.0035
Rotation	50 in.	0.0003	0.0002	0.0001
x-decenter	50 μm	0.0022	0.0026	0.0015
y-decenter	50 μm	0.0061	0.0062	0.0039
TM synthetical ΔRMS WFE (λ)		**0.0106**	**0.0100**	**0.0069**
System synthetical ΔRMS WFE(λ)		**0.6369**	**0.4699**	**0.3729**

[a]The RMS WFE values reference wavelength, $\lambda = 632.8$ nm.

Table 6. Scale Relation between System RMS WFE Increment and Off-Axis Magnitude (OM) Value

Mirror	Item	Value	System A	System B	System D
PM	Synthetical ΔRMS WFE	Value (λ)	0.6032	0.4432	0.3527
		Ratio	1.71	1.26	1
	OM	Value (mm)	350	250	200
		Ratio	1.75	1.25	1
SM	Synthetical ΔRMS WFE	Value (λ)	0.2042	0.1558	0.1210
		Ratio	1.69	1.29	1
	OM	Value (mm)	60	41	34
		Ratio	1.76	1.21	1
TM	Synthetical ΔRMS WFE	Value (λ)	0.0106	0.0100	0.0069
		Ratio	1.54	1.45	1
	OM	Value (mm)	83	65	46
		Ratio	1.80	1.41	1

4. CONCLUSIONS

In this paper, to reduce the alignment sensitivity of the unobscured optical systems, a desensitization design method of unobscured optical systems with an AOE process is proposed. By mathematical analysis, the mirror OM value is determined as a significant factor influencing system alignment sensitivity. This conclusion provides the theoretical basis for the system alignment sensitivity factor and guides us to develop the AOE desensitization design method. In the AOE desensitization design method, the OM is set as an adjustment, and the system sensitivity and image quality are set as the criteria. During the design process, the iterations of OM adjustment correction, image quality evaluation, and sensitivity analysis lead to achievement of an unobscured optical system with a lower and acceptable sensitivity. By a design example, it is demonstrated that the AOE design method is effective and practical, and the corresponding sensitivity analysis not only verifies that the OM is a significant factor influencing the system alignment sensitivity, but also verifies that there is a positive correlation relation between system sensitivity and OM value. We believe the AOE process can provide an effective and practical desensitization design method to design the unobscured optical systems with lower alignment sensitivity and robust tolerance.

Now, our design process has not been achieved automatically; some steps in AOE processes are still operated by hand. In the next stage, we aim to develop a full automaticity program and make the AOE method more efficient.

Funding. National Natural Science Foundation of China (NSFC) (61705220).

REFERENCES

1. J. M. Rodgers, "Unobscured mirror designs," Proc. SPIE **4832**, 33–60 (2002).
2. K. P. Thompson, E. Schiesser, and J. P. Rolland, "Why are freeform telescopes less alignment sensitive than a traditional unobscured TMA?" Proc. SPIE **9633**, 963317 (2015).
3. S. Li and Y. Dai, *New Technology for Manufacturing and Measurement of Large and Middle-Scale Aspheric Surfaces* (Nation Defense Industry Press of China, 2011).
4. R. Li, L. Zhang, F. Zhang, H. Xue, and X. Zhang, "Computer controlled manufacturing during fine grinding stage of highly steep off-axis asphere with large aperture," Opt. Precis. Eng. **15**, 633–639 (2007).
5. Q. Meng, W. Wang, H. Ma, and J. Dong, "Easy-aligned off-axis three-mirror system with wide field of view using freeform surface based on integration of primary and tertiary mirror," Appl. Opt. **53**, 3028–3034 (2014).
6. Q. Meng, H. Wang, K. Wang, Y. Wang, Z. Ji, and D. Wang, "Off-axis three-mirror freeform telescope with a large linear field of view based on an integration mirror," Appl. Opt. **55**, 8962–8970 (2016).
7. J. Zhu, W. Hou, X. Zhang, and G. Jin, "Design of a low F-number freeform off-axis three-mirror system with rectangular field-of-view," J. Opt. **17**, 015605 (2015).
8. T. Yang, J. Zhu, and G. Jin, "Compact freeform off-axis three-mirror imaging system based on the integration of primary and tertiary mirrors on one single surface," Chin. Opt. Lett. **14**, 60801–60805 (2016).
9. M. Beier, J. Hartung, T. Peschel, C. Damm, A. Gebhardt, S. Scheiding, D. Stumpf, U. D. Zeitner, S. Risse, R. Eberhardt, and A. Tünnermann, "Development, fabrication, and testing of an anamorphic imaging snap-together freeform telescope," Appl. Opt. **54**, 3530–3542 (2015).
10. M. Beier, J. Hartung, J. Kinast, A. Gebhardt, F. Burmeister, U. D. Zeitner, S. Risse, R. Eberhardt, and A. Tünnermann, "Fabrication of metal mirror modules for snap-together VIS telescopes," Proc. SPIE **9633**, 963313 (2015).
11. M. Beier, W. Fuhlrott, J. Hartung, W. Holota, A. Gebhardt, and S. Risse, "Large aperture freeform VIS telescope with smart alignment approach," Proc. SPIE **9912**, 99120Y (2016).
12. S. Risse, M. Beier, and J. Hartung, "Aspherical and freeform mirrors based on ultra-precise manufacturing for telescopes in the vis spectral range," Proc. SPIE **10562**, 105625T (2017).
13. T. Peschel, C. Damm, M. Beier, A. Gebhardt, S. Risse, I. Walter, I. Sebastian, and D. Krutz, "Design of an imaging spectrometer for earth observation using freeform mirrors," Proc. SPIE **10562**, 1056237 (2017).
14. J. Hartung, M. Beier, T. Peschel, A. Gebhardt, and S. Risse, "Mechanical design implementation and mathematical considerations for ultraprecise diamond turning of multiple freeform mirrors on a common substrate," Proc. SPIE **9628**, 96280U (2015).
15. T. Peschel, C. Damm, S. Scheiding, M. Beier, S. Risse, S. Nikolov, W. Holota, S. Weiß, and P. Bartsch, "Anamorphotic telescope for earth observation in the mid-infrared range," Proc. SPIE **10563**, 105631Y (2017).
16. S. Risse, S. Scheiding, M. Beier, A. Gebhardt, C. Damm, and T. Peschel, "Ultra-precise manufacturing of aspherical and freeform mirrors for high resolution telescopes," Proc. SPIE **9151**, 91510M (2014).
17. S. Risse, S. Scheiding, A. Gebhardt, C. Damm, W. Holota, R. Eberhardt, and A. Tünnermann, "Development and fabrication of a hyperspectral, mirror based IR-telescope with ultra-precise manufacturing and mounting techniques for a snap-together system assembly," Proc. SPIE **8176**, 81761N (2011).
18. K. Fuerschbach, J. P. Rolland, and K. P. Thompson, "A new family of optical systems employing φ-polynomial surfaces," Opt. Express **19**, 21919–21928 (2011).
19. K. Fuerschbach, G. E. Davis, K. P. Thompson, and J. P. Rolland, "Assembly of a freeform off-axis optical system employing three φ-polynomial Zernike mirrors," Opt. Lett. **39**, 2896–2899 (2014).
20. A. Bauer and J. P. Rolland, "Design of a freeform electronic viewfinder coupled to aberration fields of freeform optics," Opt. Express. **23**, 28141–28153 (2015).
21. D. Wang, Y. Yang, C. Chen, and Y. Zhuo, "Misalignment aberrations calibration in testing of high-numerical-aperture spherical surfaces," Appl. Opt. **50**, 2024–2031 (2011).
22. L. C. N. Scaduto, J. Sasian, M. A. Stefani, and J. C. de Neto, "Two-mirror telescope design with third-order coma insensitive to decenter misalignment," Opt. Express **21**, 6851–6865 (2013).
23. J. Meiron, "The use of merit functions based on wavefront aberrations in automatic lens design," Appl. Opt. **7**, 667–672 (1968).
24. P. D. Lin, *Advanced Geometrical Optics* (Springer, 2017).
25. Synopsys Inc., "Code V reference manual," (2012).
26. T. Yang, G. Jin, and J. Zhu, "Automated design of freeform imaging systems," Light: Sci. Appl. **6**, e17081 (2017).
27. T. Yang, J. Zhu, and G. Jin, "Starting configuration design method of freeform imaging and afocal systems with a real exit pupil," Appl. Opt. **55**, 345–353 (2016).
28. J. Reimers, A. Bauer, K. P. Thompson, and J. P. Rolland, "Freeform spectrometer enabling increased compactness," Light: Sci. Appl. **6**, e17026 (2017).
29. F. Zhang, "Fabrication and testing of optical free-form convex mirror," Chin. Opt. Lett. **13**, S12202 (2015).
30. X. Wu, J. Zhu, T. Yang, and G. Jin, "Transverse image translation using an optical freeform single lens," Appl. Opt. **54**, E55–E62 (2015).
31. Y. Zhong, H. Gross, A. Broemel, S. Kirschstein, P. Petruck, and A. Tuennermann, "Investigation of TMA systems with different freeform surfaces," Proc. SPIE **9626**, 96260X (2015).
32. J. Stock, A. Broemel, J. Hartung, D. Ochse, and H. Gross, "Description and reimplementation of real freeform surfaces," Appl. Opt. **56**, 391–396 (2017).
33. D. A. Atchison, D. H. Scott, and M. J. Cox, "Mathematical treatment of ocular aberrations: a user's guide," in *Vision Science and Its Applications*, V. Lakshminarayanan, ed. (Optical Society of America, 2000), Vol. **35**, pp. 110–130.
34. G. Catalan, "Design method of an astronomical telescope with reduced sensitivity to misalignment," Appl. Opt. **33**, 1907–1915 (1994).